New Journal of Physics
The open-access journal for physics

Subwavelength imaging with materials of in-principle arbitrarily low index contrast

Y G Ma[1], S Sahebdivan[2], C K Ong[3], T Tyc[2,4] and U Leonhardt[2,5]

[1] Center for Optical and Electromagnetic Research, State Key Laboratory of Modern Optical Instrumentation, Zhejiang University, Hangzhou 310058, China

[2] School of Physics and Astronomy, University of St Andrews, North Haugh, St Andrews KY16 9SS, UK

[3] Centre for Superconducting and Magnetic Materials, Department of Physics, National University of Singapore, Singapore 117542, Singapore

[4] Faculty of Science and Faculty of Informatics, Masaryk University, Brno, Czech Republic

E-mail: ulf@st-andrews.ac.uk

New Journal of Physics **14** (2012) 025001 (14pp)
Received 20 October 2011
Published 1 February 2012
Online at http://www.njp.org/
doi:10.1088/1367-2630/14/2/025001

Abstract. Perfect imaging with Maxwell's fish eye opens the exciting prospect of passive imaging systems with a resolution no longer limited by the wave nature of light. But it also challenges some of the accepted wisdom of super-resolution imaging and therefore has been subject to controversy and discussion. Here we describe an idea for even simpler perfect-imaging systems based on geometrical optics and prove by experiment that it works.

[5] Author to whom any correspondence should be addressed.

Contents

1. Introduction

The archetype of perfect imaging with positive refraction is Maxwell's fish eye [1–6]. It is easy to understand why Maxwell's device may focus light with unlimited precision if we consider the fact [2] that it represents the geometry of a virtual sphere—in physical space, light propagates in a medium with Maxwell's profile as if it were confined to the surface of a sphere[6] in virtual space [4]. Imagine light emission on the virtual sphere. A wave emitted at a point source on the sphere must converge with point-like precision at the antipodal point, simply due to the perfect symmetry of the sphere. The sphere thus turns the wave expanding from the point of emission into a converging wave at the image point.

It is also easy to understand why perfect imaging is possible in this case, using an argument by Feynman [8] that goes as follows [9]. Maxwell's equations of light propagation are completely time-reversible. Therefore the emission process at a point source can be completely reversed at the image, provided one crucial element is present, a source run in reverse—a drain. Otherwise the absorption at the image would not be the exact time reverse of the emission at the source. The drain at the image point is also something natural in imaging where one wishes to detect an image, for example by photochemical reactions or in a charge coupled device array. The drain represents a detector[7]. The crucial point of perfect imaging is that, given a choice of detectors in the image area, the light localizes at the correct ones.

The fact that the correct light localization naturally happens in Maxwell's fish eye is also understandable if we imagine the absorption in an array of detectors as the time reverse of the emission by a collection of point sources. Given perfect time symmetry, the light must settle down at the image points that correspond to the actual source points and avoid the ones

[6] One can also confine light on the surface of a real sphere; see the beautiful experiment reported in [7].

[7] The localization of a wave by a time-reversed emission process was beautifully demonstrated with sound waves using an active drain [10]. Note that an active drain is not necessary: in our previous microwave experiment [11] we used a passive drain—the drain only responded to the incident radiation—and obtained subwavelength resolution.

corresponding to potential source points that did not emit. In this way, a sharp image is formed with a resolution given by the cross section of the detectors and not by the wave nature of light.

Despite the simplicity and generality of these ideas and arguments, they stirred up controversy [12–23], because they challenge some of the accepted wisdom of super-resolution imaging [24]. It has been an often unquestioned mantra that perfect imaging is only possible if evanescent waves are amplified in some way. It has been firmly accepted that evanescent waves are the carriers of subwavelength details and that the near-field information is lost in the far field, as evanescent waves exponentially decay away. However, this belief is in contradiction with Feynman's general argument based on the time-reversal symmetry of Maxwell's equations [8, 9]. The near field of a point source is not lost in the far field, but rather constitutes a natural part of the emission process. If the emission is reversed in a point detector the near field naturally arises. The precise information about the point of emission is not gone; it is carried by the light wave; yet to retrieve it requires unusual imaging systems [25].

In a previous paper [11], we implemented Maxwell's fish eye for microwaves and observed subwavelength imaging. In this paper, we demonstrate an idea [25] for a modified fish-eye mirror that requires, in principle, an arbitrarily low index contrast. Such a device can be made with conventional graded-index materials. In our case, however, we used a microwave metamaterial, because of its low cost. We have demonstrated subwavelength imaging for microwaves, because microwave technology gives us a degree of detail and precision that is currently impossible in the optical range of the spectrum. In addition to demonstrating an idea for reducing the demands on the materials required for perfect-imaging systems, our experiment illustrates two fundamental points that may also become important in practice.

Firstly, we demonstrate that it is not necessary to detect the field with perfect efficiency. The undetected part of the field does not localize at the detectors with subwavelength resolution, but the detected part of the field finds its way into the right detectors. The subwavelength image appears in the detectors, but not necessarily in the field around them. However, what counts in practice is only the detected part of the field, which implies that the efficiency of the detectors is less important than their resolution.

Secondly, for the perfect imaging of light waves, ray optics seems sufficient; we only require that all light rays from any point of the source intersect at the corresponding image point, which is the defining property of an absolute optical instrument [3]. Within geometrical optics, all rays reach the image with the same phase [3], which seems to guarantee perfect imaging also in wave optics.

2. Theory

It may be surprising that geometrical optics alone is able to predict the perfect imaging of waves. Note, however, that geometrical optics goes beyond ray tracing: it is an approximative theory for the propagation of electromagnetic waves. In geometrical optics, rays serve as guiding lines for the propagation of the phase, the intensity follows their density and the polarization is parallel-transported along them [6]. Rays rule the waves: they completely dominate their behaviour, as long as geometrical optics is valid. The condition for the validity of geometrical optics is the requirement that the optical properties of the material do not vary significantly on the scale of the wavelength.

Consider the simplest nontrivial case for imaging: two-dimensional (2D) wave propagation in a planar medium, which is also the case we investigate experimentally. The electromagnetic

wave shall be polarized such that the electric field vector is orthogonal to the propagation plane. In this case, the complex Fourier component E of the electric field strength obeys the Helmholtz equation

$$\left(\nabla^2 + n^2 k^2\right) E = 0, \tag{1}$$

where n denotes the refractive-index profile, $k = \omega/c$, with ω being the (angular) frequency, and c is the speed of light in vacuum. The local wavelength is given by

$$\lambda = \frac{2\pi}{nk}. \tag{2}$$

In geometrical optics, we represent the field in terms of the amplitude $\mathcal{E}$ and phase φ as

$$E = \mathcal{E}\, \mathrm{e}^{\mathrm{i}\varphi}, \tag{3}$$

where both $\mathcal{E}$ and φ are real. Substituting the ansatz (3) in the Helmholtz equation (1) gives

$$(\nabla\varphi)^2 = n^2 k^2, \quad \nabla \cdot \left(\mathcal{E}^2\, \nabla\varphi\right) = 0, \tag{4}$$

where we ignored $\nabla^2\mathcal{E}$ in the equation for $(\nabla\varphi)^2$ on the grounds that the amplitude varies less than the phase. This term becomes important in the regions where the field becomes very strong, for instance near the source and image points. However, it turns out that it simply results in a phase shift of the wave at the point where the field is concentrated, as we will show. The relations (4) formulate the foundations of geometrical optics for our case, the 2D propagation of electromagnetic waves in planar media[8]. They describe how the refractive-index profile moulds the phase and how the phase gradient governs the transport of the field intensity. Light rays are the lines orthogonal to the phase fronts; they follow $\nabla\phi$ and obey Hamilton's equations [6]. A criterion for the validity of geometrical optics is the requirement [26]

$$|\nabla\lambda| \ll 1, \tag{5}$$

which means, according to definition (2), that the index profile ought to vary on larger scales than the wavelength (the inverse of the relative gradient $|\nabla n|/n$ should be much larger than λ).

Suppose that geometrical optics is valid and that all light rays from each point in the emission region intersect at the corresponding imaging point (figure 1). As the rays carry the complete wave, the field near the point of emission must reconstitute at the image point, provided a drain is present there. We may see this from the following argument. Close to the source point $\boldsymbol{r}_0$ and the drain at the image point $\boldsymbol{r}_0'$ the field intensity grows significantly on a scale that is smaller than the wavelength and hence also smaller than the variation of the material. Near $\boldsymbol{r}_0$ and $\boldsymbol{r}_0'$ we can thus regard the medium as being uniform, with constant refractive index n_0 and n_0', respectively. Imagine first the emission at the source. The solution of the Helmholtz equation is

$$E \sim E_0\, H_0^{(1)}(n_0 k|\boldsymbol{r} - \boldsymbol{r}_0|) \quad \text{(source)}, \tag{6}$$

where $H_0^{(1)}$ is a Hankel function (Bessel function of the third kind [27]). Near the source the field is enhanced as [27]

$$E \sim E_0 \frac{2\mathrm{i}}{\pi} \ln|\boldsymbol{r} - \boldsymbol{r}_0| \quad \text{(near field)}, \tag{7}$$

[8] For the 3D case with arbitrary polarization, see [6].

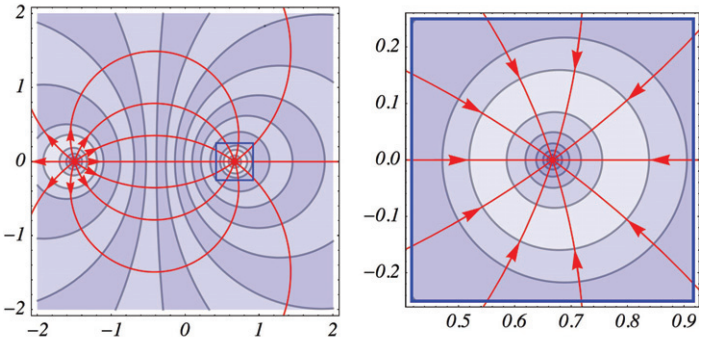

Figure 1. Geometrical optics. The picture illustrates the emission and absorption of light in the archetype of a perfect-imaging device with positive refraction, Maxwell's fish eye [4]. The contour plots display the real part of the exact solution of the Helmholtz equation, the light wave, whereas the red lines indicate the light rays—they are orthogonal to the phase fronts of the wave. The left figure shows how the rays rule the waves. The right figure focuses on the region around the imaging point; it shows a magnified plot of the blue square of the left figure. Here the light rays converge at the imaging point, but also the field intensity diverges such that geometrical optics is no longer valid. Nevertheless, the approximate solution from geometrical optics matches an exact solution around the imaging point where the medium is assumed to be uniform. The far field captured by geometrical optics seamlessly matches the near field at the detector in the focus. Therefore, geometrical optics may be used to predict perfect imaging.

but further away we see from the asymptotics of the Hankel function [27]

$$E \sim \frac{E_0\sqrt{2}}{\sqrt{\pi|\boldsymbol{r}-\boldsymbol{r}_0|}}\exp\left(\mathrm{i}n_0k|\boldsymbol{r}-\boldsymbol{r}_0|-\mathrm{i}\frac{\pi}{4}\right) \quad \text{(far field)}. \tag{8}$$

One verifies that the asymptotic formula (8) is consistent with the relations (4) of geometrical optics. Expression (6) thus describes how the near field (7) of the source is connected to the far field (8). Comparing equations (8) and (7), we also see that the transition from the near field to the far field comes with a phase shift of $\pi/4$. The field then propagates away as an outgoing wave, following the laws of geometrical optics. If, as we have assumed, all light rays from $\boldsymbol{r}_0$ focus at the image point $\boldsymbol{r}_0'$, the phase must be uniform at the image where we can regard E as the ingoing wave

$$E \sim \frac{E_0'\sqrt{2}}{\sqrt{\pi|\boldsymbol{r}-\boldsymbol{r}_0'|}}\exp\left(-\mathrm{i}n_0'k|\boldsymbol{r}-\boldsymbol{r}_0'|+\mathrm{i}\frac{\pi}{4}\right) \quad \text{(far field)} \tag{9}$$

with some complex constant E_0' that contains the amplitude and the phase of the wave approaching the image point. If, as we have also assumed, a detector is placed at the image point, the far field (9) goes over into the near field

$$E \sim E_0'\frac{2\mathrm{i}}{\pi}\ln|\boldsymbol{r}-\boldsymbol{r}_0'| \quad \text{(near field)} \tag{10}$$

of the wave at the image, because the asymptotic expressions (9) and (10) are consistent with the exact solution of the Helmholtz equation (1)

$$E \sim E_0' \, H_0^{(2)}\left(n_0' k |\boldsymbol{r} - \boldsymbol{r}_0'|\right) \quad \text{(image)} \tag{11}$$

for a uniform medium with index n_0' close to the image point (figure 1). Here $H_0^{(2)}$ is the complex conjugate of $H_0^{(1)}$. In this way, the emission and absorption are seamlessly connected to geometrical optics. Therefore, we can use geometrical optics for predicting the condition for perfect imaging. Behind this reasoning lies the idea that the near field is simply a natural part of the emission and absorption processes. Our experimental results turn out to be consistent with this concept.

3. Design

The use of geometrical optics widens the design of perfect-imaging devices. Designing perfect lenses with radial symmetry is an inverse scattering problem. This problem was probably first solved by Luneburg in his 1944 lectures on optics at Brown University and was later published in his posthumous book [2]. In 1953, Firsov [28] independently developed the same procedure for the equivalent problem in classical mechanics [29]. Here we use the notation of [30] where a visual interpretation of scattering tomography was developed; for more details, see section 8 of the textbook [6]. The only ingredient we are going to add to Luneburg's case is a mirror.

3.1. Luneburg's design problem

Consider a radially symmetric index profile $n(r)$ that extends to the radius r_0 (figure 2). We require that all rays emitted from a point at radius r_1 (with $r_1 \geqslant r_0$) are focused at an opposite point at radius r_2 (with $r_2 \geqslant r_0$ as well) as long as they hit the index profile. Consider a ray with impact parameter b. The scattering angle between the two points is

$$\chi = -\alpha_1 - \alpha_2, \quad \sin\alpha_i = \frac{b}{r_i}, \tag{12}$$

as long as $b \leqslant r_0$; otherwise the scattering angle is zero, because the ray misses the focusing index profile. The profile that implements these scattering data is given in implicit form by [6, 30]

$$n(\rho) = \exp\left(-\frac{1}{\pi}\int_\rho^{r_0} \frac{\chi \, \mathrm{d}b}{\sqrt{b^2 - \rho^2}}\right), \tag{13}$$

where the turning parameter ρ is defined as

$$\rho = nr. \tag{14}$$

The turning parameter ρ is the impact parameter b for which the trajectory has a radial turning point at r. The reconstruction formula (13) is implicit, because n is not directly expressed as a function of the radius, but in terms of the turning parameter. Not all scattering data are physically allowed, because the function $n(r)$ might be multi-valued (it may have several values of n for the same radius r). If $n(r)$ is single-valued, Luneburg's formulae (13) and (14) establish a refractive-index profile that implements the scattering data $\chi(b)$.

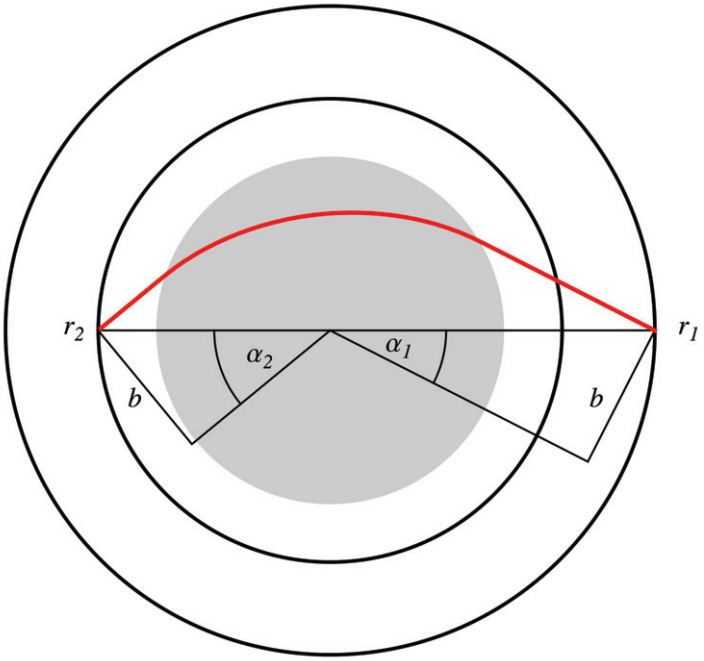

Figure 2. Luneburg's design problem. Consider light rays (red) that may pass through a spherically symmetric medium (grey). We require that all rays that do pass through the medium from radius r_1 arrive at radius r_2 exactly opposite to their starting point (meaning that the starting point and the end point lie on a straight line through $r = 0$). We characterize the rays by their impact parameters b. The impact parameter is proportional to the angular momentum and is therefore a conserved quantity, as the figure indicates. The initial and final segments of the trajectories are inclined by the angles α_1 and α_2. The drawing shows that $b = r_1 \sin\alpha_1 = r_2 \sin\alpha_2$, which is all we need to know for solving Luneburg's design problem by tomography.

3.2. Maxwell's fish eye

In order to see how Luneburg's theory works, consider the case of Maxwell's fish eye. Here the medium extends to the radius r_2 that corresponds to the equator of the virtual sphere. Light emitted at the equator should be focused on the opposite side of the equator. We thus require

$$r_2 = r_0, \quad r_2 = r_1. \tag{15}$$

In this case, $\alpha_1 = \alpha_2 = \arcsin(b/r_0)$. We use the integral

$$\int_\rho^{r_0} \frac{\arcsin(b/r_0)}{\sqrt{b^2 - \rho^2}} \mathrm{d}b = \frac{\pi}{2} \ln(1 + \sqrt{1 - (\rho/r_0)^2}) \tag{16}$$

and obtain from the reconstruction formula (13) the index profile in terms of the turning parameter:

$$n(\rho) = 1 + \sqrt{1 - (\rho/r_0)^2}. \tag{17}$$

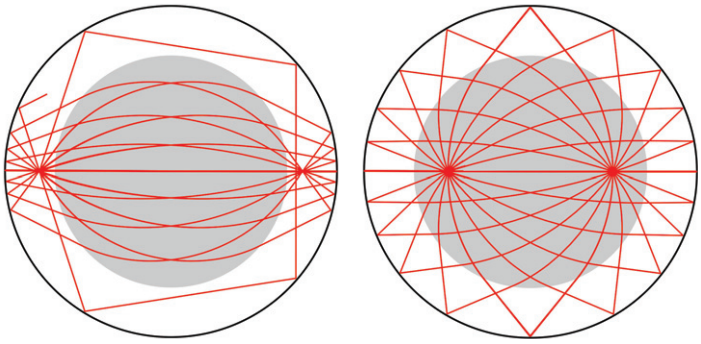

Figure 3. Modified fish-eye mirror. Left: light emitted from a point outside the focusing index profile. Not all rays are focused at the image point. Right: perfect imaging within ray optics if the light is emitted inside the index profile.

We substitute this result in definition (14) of the turning parameter and solve the resulting equation for ρ. We obtain Maxwell's profile [1]:

$$n = \frac{2}{1 + (r/r_0)^2}. \tag{18}$$

Maxwell's fish eye may act as a perfect-imaging device if we take r from 0 to infinity or if we terminate the refractive index profile at r_0, as our design method suggests, and surround it by a mirror there [4]. In this case, the refractive index ranges from 1 at r_0 to 2 at the centre.

3.3. Modified fish-eye mirror

In the following, we are going to modify Maxwell's fish eye such that the required range of the refractive index profile is reduced. We will argue that the modified device still acts as an absolute optical instrument [3] capable of perfect imaging if we surround it by a mirror.

Suppose that the two radii r_1 and r_2 in Luneburg's design problem (figure 2) are the same,

$$r_1 = r_2, \tag{19}$$

but $r_0 < r_1$, and we surround the device by a mirror at the radius r_1. Light coming from a point P on the mirror is focused on the other side and reflected, whereupon it goes through the focusing medium once more and returns to P. Consequently, light rays form close loops, provided they strike the focusing index profile. Suppose that we pick the point $\boldsymbol{r}$ inside the medium that lies on a ray trajectory. As all light rays that strike the medium form closed loops, so must all rays going through $\boldsymbol{r}$. The radial symmetry of the device implies that all these rays must also go through $-\mathbf{r}$. Therefore, a source at $\mathbf{r}$ is perfectly imaged at $-\boldsymbol{r}$ (figure 3). However, if the source is outside of the focusing profile, $r > r_0$, not all ray trajectories are closed and the image is not perfect (figure 3). In the case of the original fish-eye mirror [4], all ray trajectories are closed, because $r_1 = r_0$, no rays lie outside of the focusing medium.

3.4. Index profile

What does it take to make a modified fish-eye mirror? We obtain from the reconstruction formula (13) and relation (14) with the angles (12) and condition (19)

$$r(\rho) = \rho \exp\left(-\frac{2}{\pi}\int_{\rho}^{r_0} \frac{\arcsin(b/r_1)}{\sqrt{b^2 - \rho^2}}\mathrm{d}b\right). \tag{20}$$

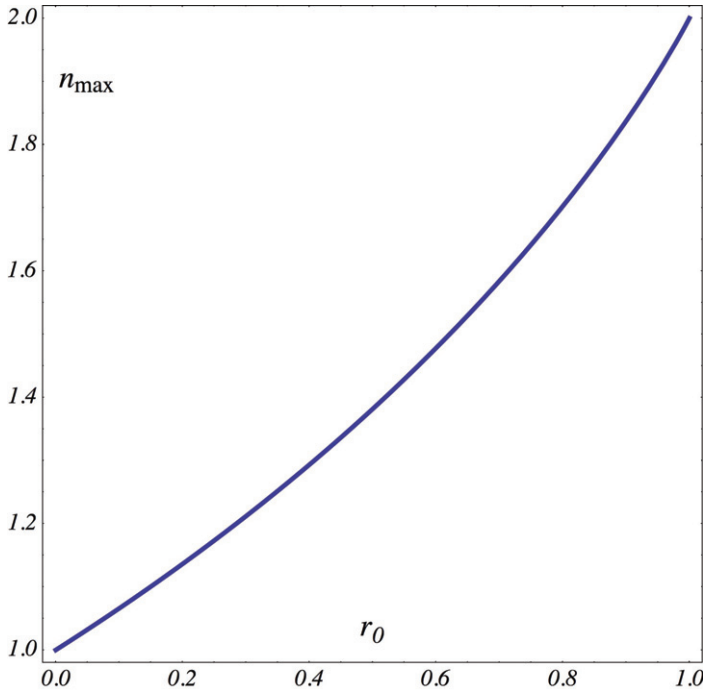

Figure 4. Maximal refractive index n_{max} required for a focusing medium with radius r_0 given in units of r_1.

The radius is a monotonically increasing function of the turning parameter ρ (seen by differentiation) and $r \leqslant \rho$. Consequently, ρ is a single-valued function of r: the index profile is physically allowed. The function $\rho(r)$ must be monotonically increasing as well. Furthermore, the function $n(\rho)$ is monotonically decreasing in ρ (seen by differentiation again) and, consequently, n is monotonically decreasing in r: the highest index value is the value at the origin with [31]

$$n_{max} = \exp\left(\frac{2}{\pi}\int_0^{r_0} \arcsin(b/r_1)\frac{db}{b}\right) = \exp\left(\frac{2}{\pi}\int_0^{r_0/r_1} \arcsin\xi\,\frac{d\xi}{\xi}\right). \tag{21}$$

With the help of this formula, one can compute by a simple numerical integration the required index range for the modified fish-eye mirror (figure 4). We see that n_{max} may be arbitrarily close to 1 for sufficiently small radii r_0.

Given the radii r_0 and r_1, the index profile itself is easily computed by storing a table of (r, ρ) values. Here ρ ranges from 0 to r_0 and r is numerically calculated according to formula (20). Then an interpolating function $\rho(r)$ is constructed from the calculated data and the index profile is computed as

$$n = \frac{\rho(r)}{r} \quad \text{for } 0 \leqslant r \leqslant r_0, \quad \text{and} \quad n = 1 \quad \text{for } r > r_0. \tag{22}$$

Figure 5 shows the profiles of the modified fish-eye mirrors depending on the ratio between the mirror radius r_1 and the radius r_2 of the material. They are modifications of Maxwell's profile (18) with n arbitrarily close to 1. We could multiply the profile by a constant n_1 and still have the same functionality, because the ray trajectories are unchanged. We thus find that the index contrast, the relative difference between n at the centre and n_1 at the rim of the

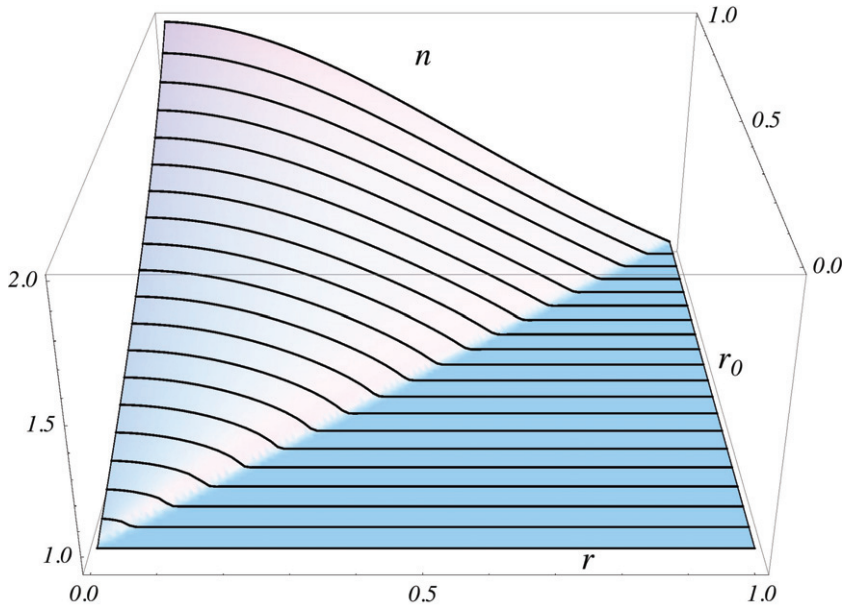

Figure 5. Index profiles $n(r)$ for focusing media with radii r_0 and r in units of r_1.

material, may be arbitrarily low. Perfect imaging is possible with materials of arbitrarily low index contrast.

4. Experiment

Our design facilitates the perfect focusing for light rays. In our theory, we use the approximation of geometrical optics to conclude that waves should be perfectly imaged. Usually, it is the wave nature of light that limits the resolution of optical instruments [3, 32]. It is therefore essential to test whether our modified fish-eye mirror does indeed exhibit subwavelength resolution. We test this on microwaves, because for microwaves we can make measurements of the field with a precision currently impossible for visible light.

4.1. Microwave device

Figure 6 shows a picture of our device. We use it for microwave radiation of 30 mm free-space wavelength (10 GHz frequency). The lens is placed inside a thin brass dish that acts as a circular mirror from the sides and ground plate at the bottom. In our device, $r_0 = 50$ mm and $r_1 = 65$ mm. It consists of 17 metamaterial rings with a height of 5 mm. The 15 inner rings are made of Rogers Ultralam®3000 circuit board patterned with 'I' or square-shaped copper structures on one side. The spacing between two neighbouring rings in the radial direction is 2.94 mm, and so is the unit size of the cells on each ring—our structures are one order of magnitude smaller than the wavelength. The two outer rings are simply made of a 0.1 mm thick mylar substrate. The inset of figure 6 shows the theoretical (blue line) and simulated (red squares) values of $\varepsilon = n^2$ for the rings of the lens. The simulated values are numerically retrieved from the scattering parameters of a stack of planar metamaterial sheets with given patterns [33].

In our experiment, the lens is placed inside a parallel-plate waveguide mounted on a flat stage driven by a computer-controlled xy step motor [11, 33, 34]. With the movable waveguide

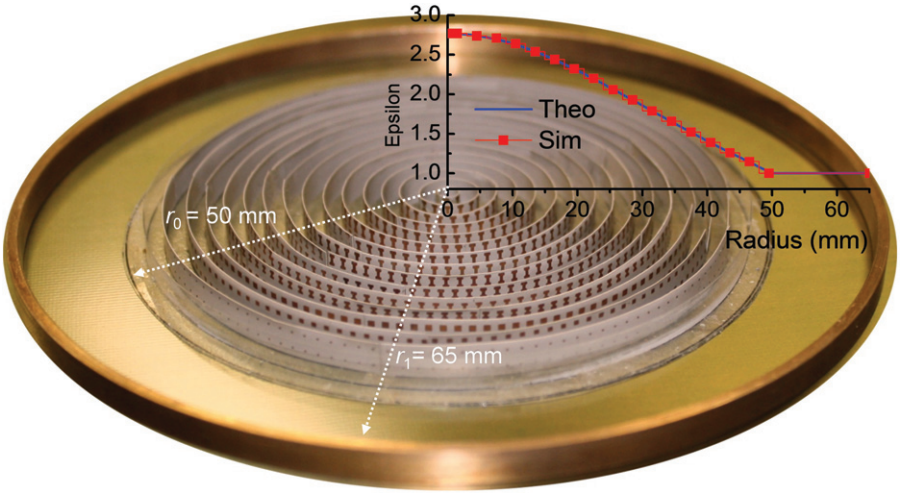

Figure 6. Microwave imaging device. The lens sits in a brass dish that serves both as a circular mirror and a ground plate. The modified fish-eye profile is produced by a microwave metamaterial made of patterned circuit board. The inset shows the theoretical curve of $\varepsilon = n^2$ versus the simulation results for the metamaterial layers.

we can scan the field through a scanning cable. The scanning resolution is given by the step size, 1 mm. For scanning we use a coaxial cable connected to a vector network analyser (HP 8722D) that also synthesizes the microwave radiation we inject into the chamber. As sources and drains we use coaxial cables as well. All cables are Teflon-filled and have 1.68 mm outer shell diameter and 0.5 mm inner core diameter. By adjusting the exposure of the inner core we control the cross section of the cables; the scanning cable has zero exposure and the source and drain cables have an exposure length of 4.8 mm.

We observed in our experiments that the cross section of the cables is important for the detection in perfect imaging. We believe that this fact can be explained as follows. Due to the granularity of our metamaterial, the electromagnetic wave cannot localize below a certain length scale. If the cross section is smaller than this scale, as the cross section of the scanning cable certainly is, one cannot extract sufficient radiation from the field for forming a subwavelength image—the scanning cable simply scans the field and does not alter it significantly. The exposure length of the sources and outlets was optimized for maximal field localization, which probably means that it was optimized for reaching the cross section that matches the localization length in our device.

4.2. Measurements

The resolution of imaging is best demonstrated by placing two sources in the device. If the sources appear as separate peaks in the image we may claim to be able to resolve them. Figure 7(a) shows the scheme of our experiment. On the yellow dashed circle we place two sources a distance of 0.2λ apart, where λ is the local wavelength (2). Opposite to the sources we insert nine outlet cables at 0.1λ distance from each other. We scan the field at the outlets. We also measure the field going through the outlets as follows. All outlets but one are terminated by

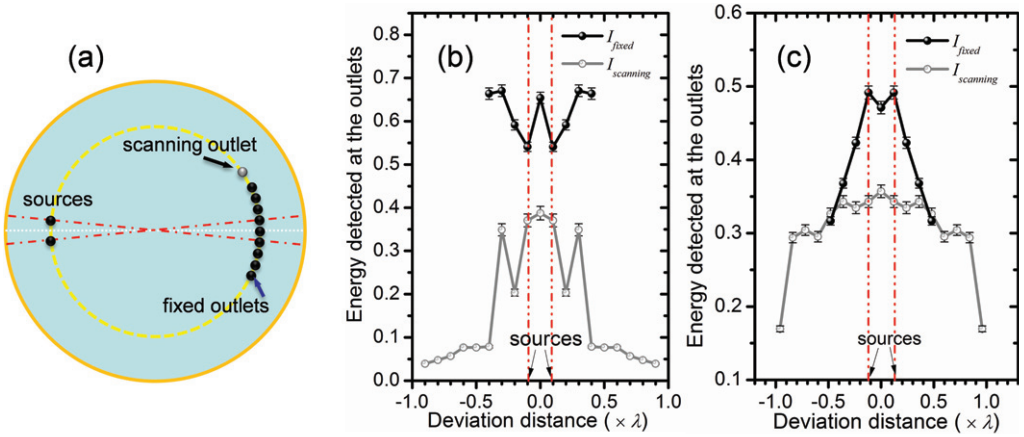

Figure 7. Imaging experiments. (a) Schematic diagram of the experiments. Two sources are placed on the yellow dashed circle. The distance between the sources is 0.2λ, where λ is the local wavelength. An ordinary instrument would not be able to resolve the two sources, but here we image them with a modified fish-eye mirror (figure 6). The image is detected by nine outlets also indicated on the yellow dashed circle. We average over four runs of the experiments and obtain statistical error bars. (b) Imaging outside of the lens, which corresponds to the left picture of figure 3 where we do not expect perfect imaging. We record the throughput through the outlets (black dots) and scan the field along them (grey dots). Our measurements show that the two sources are not resolved. (c) Imaging within the lens where perfect imaging is possible. The scanned field (grey dots) does not exhibit marked peaks at the expected image points, but the throughput (black dots) distinguishes the two sources, thus demonstrating subwavelength imaging with a modified fish-eye mirror.

impedance-matched absorbers; the one outlet is connected to the detecting port of the vector network analyser where the amplitude is measured. The throughput through each outlet is measured one by one by repeating the experiment within the relevant outlet connected. In this way we demonstrate the effect of a multiple-detector array with just one life detector at a time. We repeat the entire experiment four times for reducing statistical fluctuations. We investigate two cases: sources and detectors outside of the lens (for $r_0 < r < r_1$) and inside the lens (for $r < r_0$) that correspond to the ray trajectories illustrated in figure 3. Figure 7(b) shows the results for the attempted imaging outside of the lens and figure 7(c) the results when the sources and detectors are inside the lens area. In both cases the scanned field (grey dots) does not resolve the two sources. However, when the imaging occurs inside the lens the measurements of the throughput (black dots) resolve the sources, despite the fact that they are separated by the fraction 0.2 of the local wavelength.

4.3. Discussion

In our previous demonstration of subwavelength imaging with Maxwell's fish eye [11], we clearly observed the localization of the field at the image outlets, but with the modified fish-eye mirror we were not able to observe this effect. The subwavelength image appeared in

the detected throughput; yet there it is also significantly less clear than in the original fish eye [11]. These findings suggest that the modified fish eye depends in a more sensitive way on inaccuracies in its implementation, in particular on the structure size of the material used (2.94 mm in our case). One might expect that the less the demands on the index range become, the higher the requirements on the accuracy of the profile. Graded refractive-index materials or tapered waveguides [35, 36] instead of metamaterials might not suffer from problems caused by the granularity of a metamaterial.

The fact that the subwavelength image appears in the detected intensity profile, despite its absence in the field localization, is consistent with the idea that perfect imaging is not sensitive to the detection efficiency but rather to the resolution of the detectors (and the structure size of the material). If the detection is not perfect we can imagine the field as a mixture of an undetected field and the field that has undergone detection. The undetected field does not localize with subwavelength resolution and so does not form sharp spikes, but only the detected field does. In our case we could not observe this feature with the fairly crude implementation of a modified fish-eye mirror by a circuit-board metamaterial. However, in the detected intensity the undetected field is missing—by definition—and so the image becomes sharper. This aspect appears to have made it possible for us to resolve the two sources that were 0.2λ apart, despite the limitations of our device. As the detection of an image is the very point of imaging, we can claim to have observed subwavelength resolution.

Our measurements also show that subwavelength details only appear in the detected image in the case when all the rays are focused, i.e. when the device acts as an absolute instrument [3]. They illustrate the two ingredients for perfect imaging with positive refraction—the perfect focusing of light rays and the detection of the image.

5. Summary

Our theory suggests that absolute optical instruments [3] are possible with materials of arbitrarily low index contrast. We argued that such devices image with a resolution no longer limited by the wave nature of light. In practice, the resolution is rather limited by the cross section of detectors and the granularity of the material used. We performed a microwave experiment that supports these ideas, where we demonstrate the resolution of subwavelength details with a device that has a lower index contrast than Maxwell's fish eye. If these concepts are indeed correct they may pave the way for practical perfect-imaging devices where imaging matters most, for visible light.

Acknowledgments

We thank Aaron Danner, Andrea Di Falco, Lucas Gabrielli, Yang Hao, Simon Horsley, Susanne Kehr, Michal Lipson, Thomas Philbin and Gunther Uhlmann for discussions. MYG acknowledges support from the Key National Science Fund of China (no. 60990322 and no. 91130004) and the Fundamental Research Funds for the Central Universities of China. SS is funded by SORSAS and the University of St Andrews. CKO is supported by the MOE academic research fund of Singapore. TT and UL are both funded by the QUEST programme grant of the Engineering and Physical Sciences Research Council; TT is also funded by the grants MSM0021622409 and MSM0021622419 and UL is supported by the Royal Society.

References

[1] Maxwell J C 1854 *Cambridge and Dublin Math. J.* **8** 188
[2] Luneburg R K 1964 *Mathematical Theory of Optics* (Berkeley, Los Angeles, CA: University of California Press)
[3] Born M and Wolf E 1999 *Principles of Optics* (Cambridge: Cambridge University Press)
[4] Leonhardt U 2009 *New J. Phys.* **11** 093040
[5] Leonhardt U and Philbin T G 2010 *Phys. Rev.* A **81** 011804
[6] Leonhardt U and Philbin T G 2010 *Geometry and Light: The Science of Invisibility* (Mineola, NY: Dover)
[7] Schultheiss V H, Batz S, Szameit A, Dreisow F, Nolte S, Tünnermann A, Longhi S and Peschel U 2010 *Phys. Rev. Lett.* **105** 143901
[8] Feynman R P, Leighton R P and Sands M 2006 *The Feynman Lectures on Physics* vol II (San Francisco, CA: Addison-Wesley)
[9] Quabis S, Dorn R, Eberler M, Glöckl O and Leuchs G 2000 *Opt. Commun.* **179** 1
[10] de Rosny L and Fink M 2002 *Phys. Rev. Lett.* **89** 124301
[11] Ma Y G, Sahebdivan S, Ong C K, Tyc T and Leonhardt U 2011 *New J. Phys.* **13** 033016
[12] Blaikie R J 2010 *New J. Phys.* **12** 058001
[13] Leonhardt U 2010 *New J. Phys.* **12** 058002
[14] Guenneau S, Diatta A and McPhedran R C 2010 *J. Mod. Opt.* **57** 511
[15] Sun F and He S 2010 *Prog. Electromagn. Res.* **108** 307
[16] Sun F, Ge X and He S 2010 *Prog. Electromagn. Res.* **110** 313
[17] Kinsler P 2010 *Phys. Rev.* A **82** 055804
[18] Merlin R 2010 *Phys. Rev.* A **82** 057801
[19] Leonhardt U and Philbin T G 2010 *Phys. Rev.* A **82** 057802
[20] Leonhardt U and Sahebdivan S 2011 *J. Opt.* **13** 024016
[21] Merlin R 2011 *J. Opt.* **13** 024017
[22] Kinsler P and Favaro A 2011 *New J. Phys.* **13** 028001
[23] Leonhardt U 2011 *New J. Phys.* **13** 028002
[24] Pendry J B 2000 *Phys. Rev. Lett.* **85** 3966
[25] Leonhardt U, Tyc T, Gabrielli L H and Lipson M 2011 Imaging device and method *PCT Patent* WO/036-469 A1
[26] Landau L D and Lifshitz E M 1977 *Quantum Mechanics* (Oxford: Butterworth-Heinemann)
[27] Erdélyi A, Magnus W, Oberhettinger F and Tricomi F G 1981 *Higher Transcendental Functions* vol II (New York: McGraw-Hill)
[28] Firsov O B 1953 *Zh. Eksp. Teor. Fiz.* **24** 279
[29] Landau L D and Lifshitz E M 1982 *Mechanics* (Oxford: Butterworth-Heinemann)
[30] Hendi A, Henn J and Leonhardt U 2006 *Phys. Rev. Lett.* **97** 073902
[31] Demkov Yu N, Ostrovsky V N and Berezina N B 1971 *Sov. Phys.—JETP* **33** 867
[32] Abbe E 1873 *Arch. Mikrosk. Anat.* **9** 413
[33] Ma Y G, Ong C K, Tyc T and Leonhardt U 2009 *Nature Mater.* **8** 639
[34] Zhao L, Chen X and Ong C K 2008 *Rev. Sci. Instrum.* **79** 124701
[35] Smolyaninova V N, Smolyaninov I I, Kildishev A V and Shalaev V M 2010 *Opt. Lett.* **35** 3396
[36] Di Falco A, Kehr S C and Leonhardt U 2011 *Opt. Express* **19** 5156